Patient's dermal fibroblasts as disease markers for visceral myopathy

Federica Viti [a,*], Francesca Micaela Pramotton [b,c], Michela Martufi [a,g], Raffaella Magrassi [a],
Nicoletta Pedemonte [d], Mario Nizzari [a], Francesca Cella Zanacchi [e], Benedetta De Michele [a],
Manuela Alampi [f], Martina Zambito [g], Giuseppe Santamaria [h], Adriana Bajetto [g], Sabah Sardar [k],
Valeria Tomati [d], Paolo Gandullia [i], Costanza Giampietro [b,c], Tullio Florio [g,j],
Francesco Beltrame [f], Massimo Vassalli [k], Isabella Ceccherini [h]

[a] *Istituto di Biofisica – Consiglio Nazionale delle Ricerche, Via De Marini 16, 16149 Genova, Italy*
[b] *EMPA, Swiss Federal Laboratories for Materials Science and Technology, Ueberlandstrasse 129, 8600 Dübendorf, Switzerland*
[c] *ETH Zurich, The Institute for Mechanical Systems, Leonhardstrasse 21, 8092 Zürich, Switzerland*
[d] *UOC Genetica Medica, IRCCS Istituto Giannina Gaslini, Via Gaslini 5, 16147 Genova, Italy*
[e] *Department of Physics, University of Pisa, Largo Bruno Pontecorvo 3, 56127 Pisa, Italy*
[f] *Department of Informatics, Bioengineering, Robotics and Systems Engineering, University of Genoa, Viale Causa, 13, 16145 Genova, Italy*
[g] *Dipartimento Medicina Interna, Sezione di Farmacologia, Università di Genova, viale Benedetto XV, 2, 16132 Genova, Italy*
[h] *UOSD Laboratorio di Genetica e Genomica delle Malattie Rare, IRCCS Istituto Giannina Gaslini, Via Gaslini 5, 16147 Genova, Italy*
[i] *UOC Pediatric Gastroenterology and Digestive Endoscopy, IRCCS Istituto Giannina Gaslini, Via Gaslini 5, 16147 Genova, Italy*
[j] *IRCCS Ospedale Policlinico San Martino, Largo rosanna benzi 10, 16132 Genova, Italy*
[k] *Centre for the Cellular Microenvironment, James Watt School of Engineering, University of Glasgow, Oakfield avenue, G128LT Glasgow, UK*

A R T I C L E I N F O

A B S T R A C T

Visceral myopathy (VSCM) is a rare genetic disease, orphan of pharmacological therapy. VSCM diagnosis is not always straightforward due to symptomatology similarities with mitochondrial or neuronal forms of intestinal pseudo-obstruction. The most prevalent form of VSCM is associates with variants in the gene *ACTG2*, encoding the protein gamma-2 actin. Overall, VSCM is a mechano-biological disorder, in which different genetic variants lead to similar alterations to the contractile phenotype of enteric smooth muscles, resulting in the emergence of life-threatening symptoms. In this work we analyzed the morpho-mechanical phenotype of human dermal fibroblasts from patients affected with VSCM, demonstrating that they retain a clear signature of the disease when compared with different controls. We evaluated several biophysical traits of fibroblasts, and we show that a measure of cellular traction forces can be used as a non-specific biomarker of the disease. We propose that a simple assay based on traction forces could be designed to provide a valuable support for clinical decision or pre-clinical research.

1. Introduction

Gastrointestinal (GI) motility disorders are a major medical challenge, ranging from common and generally benign conditions, to rare and potentially life-threatening diseases [1]. Chronic intestinal pseudo-obstruction (CIPO) represents the most severe form of GI motility disorder and is characterized by failures in the propulsion of the intestinal content due to inefficient peristalsis [2]. VSCM is the myogenic form of CIPO, a rare genetic disorder, orphan of therapy, clinically characterized by intestinal, bladder, and uterine dysfunction [3]. Different spectra of severity have been described for VSCM, ranging from variable degrees of

isolated intestinal pseudo-obstruction with neonatal (mostly), infantile or adult onset, to the association with other manifestations such as malrotation, urinary involvement (Hollow Visceral Myopathy), and the most severe Megacystis Microcolon Intestinal Hypoperistalsis Syndrome [4,5]. VSCM diagnosis currently relies on clinical evidence and genetic investigation. The most recurrent genetic causes of VSCM are autosomal dominant missense variants in the γ-enteric smooth muscle actin gene (ACTG2) [6] which account for approximately 45 % of VSCM cases. *ACTG2* encodes the γ-2 actin (gSMA), predominantly expressed in intestinal and urogenital smooth muscle cells (SMCs) [7]. The correct expression of *ACTG2* gene is crucial to maintain the structural and

Table 1
List of samples considered in the study.

Pseudo-anonymized code	Description
1	Control: cell line from non-CIPO patient, anorectal malformation
2	Control: cell line from non-CIPO patient, hypospadias
3	Control: cell line from non-CIPO patient, hemato-immunological disorder
4	Control: cell line from non-CIPO patient, apparently healthy individual
5	Control: cell line from non-CIPO patient, apparently healthy individual
6	Control: cell line from patient showing aganglionic megacolon (Hirschsprung) without variants in RET gene
7	Control: cell line from patient showing aganglionic megacolon (Hirschsprung) carrying p.R287W variant in RET gene
8	Control: cell line from patient showing aganglionic megacolon (Hirschsprung) without variants in RET gene
9	Cell line from $ACTG2^{R257C}$ VSCM (severe myogenic CIPO) patient
10	Cell line from $ACTG2^{R257C}$ VSCM (severe myogenic CIPO) patient
11	Cell line from $ACTG2^{R257C}$ VSCM (severe myogenic CIPO) patient
12	Cell line from $ACTG2^{R38H}$ VSCM (mild myogenic CIPO) patient

The significance of the green ones are non-CIPO controls, the yellow ones are HSRC controls, and the red are VSCM (as in the rest of the paper).

functional integrity of smooth muscle, and alterations of this gene lead to a reduction of muscle contraction ability [8]. Distinct *ACTG2* variants are implicated in different VSCM forms, most of them affecting an arginine residue, such as changes at arginine codons 257 (R257C) [8] and 178 (R178H, R178C, R178L) [6,9], which are responsible for severe forms of the disease. Also milder VSCM forms exist, such as those involving the R38 (R38H) and R40 (R40C) residues, often displaying a late onset with familial recurrence [6,9–11]. Rare homozygous loss of function variants in the *MYH11, MYL9, LMOD1, MYLK* genes [12–15], and in *ACTG2* itself [9], were also found in a few consanguineous families.

This disabling genetic disease presents two pressing unmet medical needs. On one side, a rapid and correct diagnosis is required for the timely and suitable treatment of the patients, especially in the absence of the most common associated genetic variants. On the other side, the identification of VSCM pharmacological treatments represents a fundamental step towards the improvement of life perspectives of VSCM-affected patients.

Knowledge of the phenotype of cells carrying causative variants represents a useful resource to bridge genetic and clinical observations. The clinical and genetic background of VSCM points towards the involvement of aberrant mechanobiological traits, therefore morphological and mechanical features are expected to offer a useful proxy of the underlying pathology. In fact, morphological and mechanical properties of living cells are associated with their structural characteristics and, consequently, with their functional state [16–24]. The investigation of morpho-mechanical features in the context of a disease presenting clear impairment of mechanical components, such as the intestinal peristalsis, and the crucial involvement of the visceral smooth muscle actin, part of the cytoskeleton thus impacting on cell shape and mechanics, can provide novel insights on the disease. This hypothesis has been recently considered by Hashmi et al., who expressed the R257C mutant form of gSMA in primary human intestinal smooth muscle cells and evaluated several morpho-mechanical aspects such as the organization of the cytoskeleton, the contractility, and the migratory ability of transfected cells [3].

In the present paper, we describe a comprehensive cell morpho-mechanical study on primary dermal fibroblasts from VSCM-affected patients, compared to control fibroblasts from non-VSCM individuals. This study represents the first attempt to investigate the morpho-mechanical phenotype of cells from VSCM patients, to identify bio-markers useful in novel functional tests for speeding up the diagnostic

procedure and for studying novel pharmacological therapies. The choice of fibroblasts as model for this work is based on their ease of collection and management, compared to other cell types, which represents an advantage when considering the translation of results into the diagnostic path. Finally, detectable amounts of *ACTG2* RNA as well as gSMA protein have been demonstrated in dermal fibroblasts, thus making these cells not only a suitable but also a reliable model of the disease.

2. Methods

2.1. The experimental design

Overall, 12 primary skin fibroblast cell lines were collected, and reported here through pseudo-anonymized codes, from 1 to 12 (Table 1).

Patients diagnosed with VSCM were collected and screened for variants of the *ACTG2* gene, as already described [9,10]. Four of these (namely 'VSCM' cases, lines 9-12) were selected based on availability of fibroblasts in the biobank of the Giannina Gaslini Institute, in Genova (informed consents collected from families and study protocol approved by the "Comitato Etico Regionale della Liguria" - n. registro CER Liguria: 269/2021 - DB id 11485). In particular, primary dermal fibroblasts from the following patients were used in this work: three unrelated VSCM patients with a defective *ACTG2* gene carrying the p.R257C variant (namely 'severe VSCM' cases and identified as $ACTG2^{R257C}$, lines 9–11), and one with the p.R38H variant (namely 'mild VSCM' case and identified as $ACTG2^{R38H}$, line 12). Other fibroblasts were used as controls (namely 'all controls', lines 1–8), from non-CIPO patients and from patients with Hirschsprung disease, a developmental disorder of the enteric nervous system resulting in megacolon due to congenital aganglionosis in distal tracts of different length of the bowel [25,26].

In particular, 'non-CIPO controls' (lines 1–5) were selected from those available in the historical cell repository of the Laboratory of Genetics and Genomics of Rare Diseases of Gaslini Institute in Genoa, Italy, no one suffering from any intestinal dysmotility. Moreover, taking into account the similarity in the intestinal symptoms but not in genetics, three patients affected with Hirschsprung disease (namely 'HSCR', lines 6–8) were included in the study. These samples are instrumental to draw a wider correlation between chronic intestinal pseudo-obstruction symptoms and bio-mechanical endpoints. HSCR patients reported in the manuscript underwent genetic characterization at the RET locus (Table 1).

Overall, most of the donors are in the pediatric age, although some samples come from older patients (control fibroblasts line 3,4,5). We monitored the growth of cells during culturing not observing significant differences (data not shown).

The characterization techniques regarded the evaluation of cellular migration ability, traction force, elasticity, morphology, and cytoskeleton organization. The results of the parameters obtained from the tests were first analyzed based on their ability in distinguishing cells from VSCM patients' and 'all controls'. When the hypothesis under study was not satisfied, all forms of CIPO (both myogenic and neurogenic, VSCM + HSCR) were compared to the 'non-CIPO controls'.

Patients' dermal fibroblasts showed *ACTG2* mRNA expression (see Supplementary Materials).

2.2. Cell culture treatments

Fibroblasts were cultured in RPMI medium, supplemented with 10 % fetal bovine serum, PenStrep 1 % and glutamine 1 % and were maintained at 37 °C in a 5 % CO2 incubator in a humidified atmosphere. In all tests, cells were evaluated at similar passage (between passage 3 and 5). In order to obtain homogeneous performances over the whole cell population, a synchronization protocol was applied consisting in total serum depletion on adherent, non-confluent cells for 18 h, followed by serum administration to enable the simultaneous resumption of the normal cellular activity. To this end, cells were washed first in PBS, then in PBS-Albumin 3 %, and finally again in PBS. Synchronization was applied to cells undergoing all tests, except for the migration test. In this case, in order to analyze only the contribution of cell migration and exclude the proliferation component, a proliferation suppression reagent was administered (see further).

2.3. Cell elasticity measurements

Single cell stiffness measurements were performed using a Chiaro system (Optics11Life, NL), a nanoindentation device based on a ferruletop with interferometric read-out that enables high resolution force measurements in liquid environment [27]. The experimental protocol to operate the Chiaro nanoindenter is very similar to what is required for the more widely adopted atomic force microscope (AFM) and the data can be analyzed through the same approach [27,28]. In brief, the force is measured while moving the tip towards the sample and the corresponding $F(Z)$ curve is recorded. The Chiaro device is mounted on a holographic microscope (HoloMonitor 3, Phase Holographic Imaging PHI AB, Sweden) with phase-contrast mode that allows to precisely target individual cells with the tip. Experiments were carried out with a constant approach speed of 2.5 μm/s using a soft cantilever (stiffness 0,025 N/m) and a spherical tip with a radius R of 3 μm to avoid cell damage and to guarantee a definite contact area. The mechanical properties of the cells were calculated by fitting the indentation curve with the Hertz model [29,30] up to a maximum indentation of 300 nm, selected to be smaller than 10 % of the thickness of the cell [31]. To calculate the contact-point we used a threshold method [28], keeping the same parameters for all datasets. The analysis was performed using a dedicated python software which is free and available under open source license [32] (https://github.com/CellMechLab/nanoindentation.git). Each experiment was performed in 3 replicates. At least 100 force-distance curves were acquired for each condition.

2.4. Wound healing assay

Cell migration parameters were evaluated through the wound healing assay (also known as scratch test), a standard in vitro technique for probing collective cell migration in two dimensions. To create a cell-free area in a confluent monolayer, 2-wells inserts (Culture-Insert 2 Well in μ-Dish 35 mm, IBIDI GMBH) were used, which guarantee homogeneity in wound more than the manual scratch. The exposure to the cell-free area induces the neighboring cells to migrate into the gap [33]. In order to exclude cell proliferation contribution to healing, 18 h before the start of the scratch test, fibroblasts were treated with 10 μM AraC (Cystosine β-D-Arabinofuranoside), an antineoplastic and antiviral agent, able to selectively inhibit DNA synthesis [34], thus blocking the mitotic process [35,36] without affecting RNA synthesis [37]. Pinpointing the exact wound-closure event is an operator-dependent choice [38]: therefore, image acquisition for all experiments was performed during 31 h ($t = 0$ h,4 h,8 h,16 h,20 h,24 h,28 h,31 h), independently of when the closure occurred. Images were captured using a transmission light microscope (Nikon Eclipse Ni; 4× objective) equipped with a digital camera. Cell invasion of the free area was differentially evaluated, customizing an existing ImageJ plugin [39], by comparing time point results with the initial free area. Two quantitative parameters were obtained from this analysis: the wound closure percentage and the cell migration rate (a measure of the speed of the collective motion of the cells) [33,40].

2.5. Cell traction force microscopy

For the measurement of traction forces exerted by fibroblasts, cTFM substrates were used [41]. A triangular pattern of red quantum dots (QD) disk-shaped layers of diameter ~200 nm was printed, by means of electrohydrodynamic nanodrip printing [42], in monocrystalline arrays with spacing of 3 μm, on the surface of a silicon substrate (CY52–276, 9:10 mixing ratio, DOWSIL - USA) [43], yielding an elastic modulus of 12.6 kPa. Then, substrates were sterilized and coated with fibronectin. Cells were seeded at low density and incubated for 18 h. Adhering cells generated deformations of the substrate, which were captured as distortions of the fluorescent nanodisc matrix. The subpixel detection of the QD nanodisc center was followed by computational reconstruction of the triangular mesh. From the displacement field, the surface tractions were reconstructed using finite element analysis, as previously reported [44]. Then, results were normalized by projected cell area to obtain total force of the cell [45,46]. Images were acquired on at least 3 replicates/condition. Quantum dots deformation was acquired using an inverted microscope equipped fluorescence. Images were collected using high magnification oil objectives (40× or 60×).

2.6. Digital holography

Digital holography microscopy (DHM) was exploited to identify morphological and texture features of the cell. DHM is a quantitative phase imaging, label free technique, used to evaluate single cell 2D and 3D morphological features [47]. It is based on interference phenomenon: the final image is an interference image resulting from the interaction between a reference wave and the wave passing through the sample, which introduces a phase delay. Each value depends on the cell and medium refractive index: the latter is acquired in the setup calibration phase, while the value of cell refractive index was considered to be 1,38 [48]. The Holomonitor M3 digital holography microscope (Phase Holographic Imaging PHI AB, Sweden) was used to acquire data. At least three replicates per sample were analyzed, obtaining >70 single cell images per sample from 35 mm Petri dish plated, low-confluence cells. Image analysis was performed through HStudio software (Phiab, SE), which allowed semi-automatic cell segmentation and successive extraction of 32 quantitative morphological properties from single cells (such as area, perimeter, volume, thickness, roughness, texture, eccentricity) [49,50].

2.7. Cytoskeletal organization

Fibroblasts were plated (10,000 cells/well) on clear-bottom 96-well black microplates suitable for high-content imaging. After 24 h, when reaching 50 % plate confluence, cells were washed with PBS and fixed in 10 % neutral buffered formalin for 10 min at room temperature (RT).
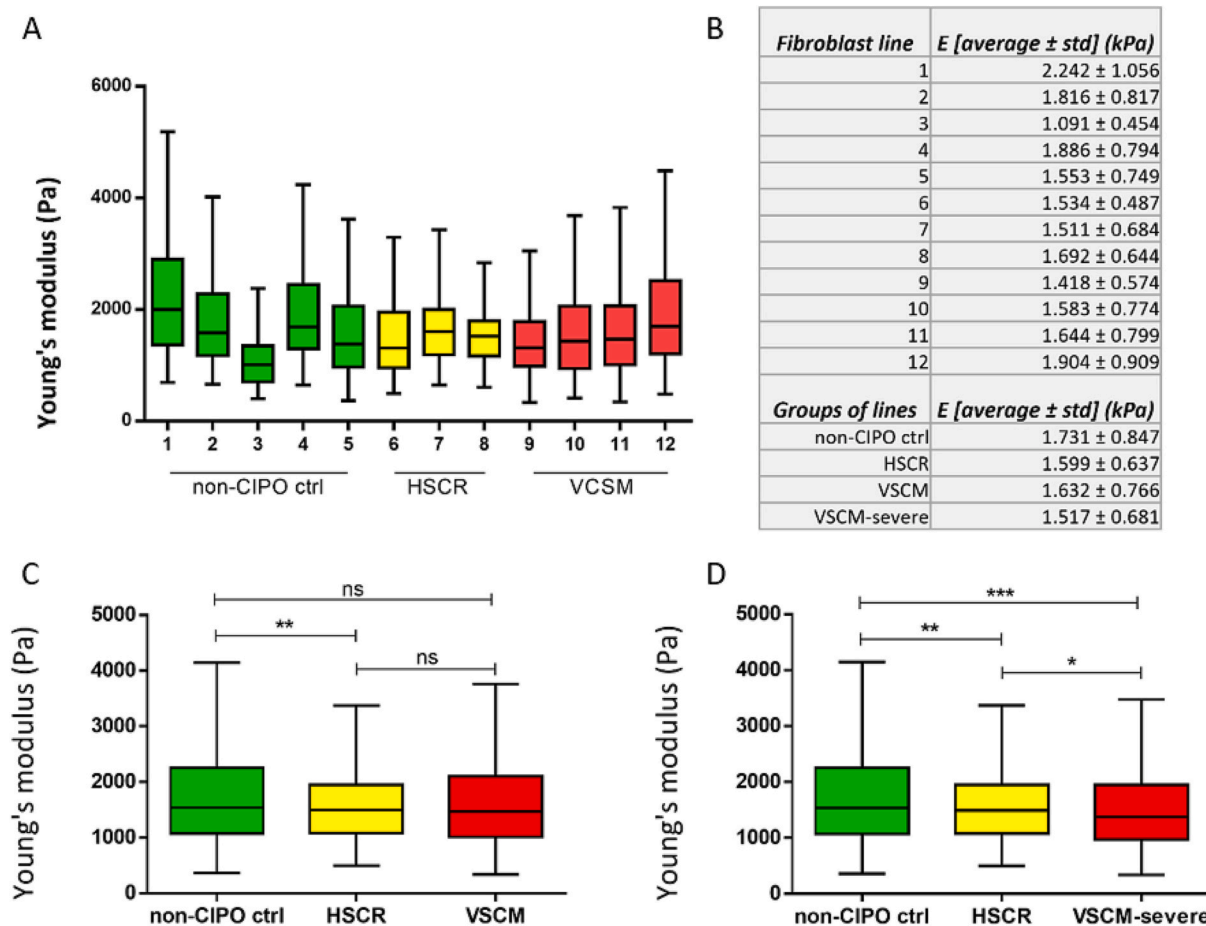
Fig. 1. Young modulus of different cell lines and average values of different groups of samples. A. single sample plot. B. quantitative data. C. non-CIPO ctrl (5 samples) versus HSCR cases (3 samples) versus VSCM cases (4 samples). D. non-CIPO ctrl (5 samples) versus HSCR cases (3 samples) versus severe VSCM cases (3 samples). Each experiment was performed in 3 replicates. At least 100 force-distance curves were acquired for each condition. *P*-value were obtained through Kolmogorov–Smirnov test for cumulative distributions.

Then, cells were permeabilized with Triton X-100 0.1 % in PBS for 10 min and then blocked with blocking buffer (5 % FBS in 0.1 % Triton X-100/PBS) for 20 min. Fibroblasts were incubated with primary polyclonal anti-ACTG2 antibody (1:200; Abcam, ab231802) at 4 °C overnight. The following day, cells were washed with PBS and incubated with a secondary anti-rabbit IgG antibody coniugated to AlexaFluor 488 (1:250; Thermo Fisher Scientific, A21206), at RT for 1 h. Actin filaments (F-actin) were labeled using phalloidin conjugated to Alexa Fluor 647 (1:50; Thermo Fisher Scientific, A30107). Cell nuclei were counterstained with Hoechst 33342. High-content imaging was performed using an Opera Phenix (PerkinElmer) high-content screening system. Wells were imaged in confocal mode, using a 40× water-immersion objective. AlexaFluor 488 signal was laser-excited at 488 nm and the emission wavelengths were collected between 500 and 550 nm. Phalloidin signal was laser-excited at 640 nm and the emission wavelengths were collected between 650 and 760 nm. Excitation and emission wavelengths for visualization of Hoechst 33342 signal were 405 and between 435 and 480 nm, respectively.

Analysis of the signal texture and ACTG2 spots were performed using the PhenoLogic machine-learning algorithm included in the Harmony software (version 4.9) of the Opera Phenix high-content system. Analysis of signal texture was based on evaluation of Haralick [51] and Gabor [52] features, two subsets of well-known parameters, included in the Harmony software of Opera Phenix. For each cell population, a minimum number of six independent regions, each one measuring 990 × 1320 μm (from six different biological replicates) were considered for the analysis, having similar cell density and distribution.

To quantify the orientation and anisotropy of cytoskeletal actin filaments, images of single fibroblasts stained with phalloidin conjugated with Alexa Fluor 647 were selected. A method [53] previously used to quantify the heterogeneity in microtubule orientations in plant tissues [54] was applied. The quantification of the main orientation and alignment of the fibrillar structures can be accessed by computing the nematic tensor (commonly used to describe liquid crystals) on the basis of the gradient of intensity levels, used to identify a unit vector locally tangent to the fibril. More specifically, circular statistics was used, adapted to directional data, to analyze the properties of the tangent direction over the region of interest. To access whether the fibrils are well ordered, the fibril anisotropy was evaluated, defining a score by computing the circular variance of the tangent direction. With this approach an anisotropy value of 0 is expected for purely isotropic arrays (no order) and anisotropy values of 1 is expected for parallel fibrils (purely anisotropic arrays). Cell borders were manually excluded using a conventional image processing software (ImageJ) to avoid artifacts and reduce errors in the cytoskeletal anisotropy estimation. Anisotropy values were then calculated for each single cell using the open access software Fibril Tool (https://github.com/marionlouveaux/FibrilTool_Batch).

2.8. Statistics

Experiments were carried out at least in technical triplicates. Most of the results obtained are reported *per* fibroblast line. When cumulative, results are presented through their average values and related standard
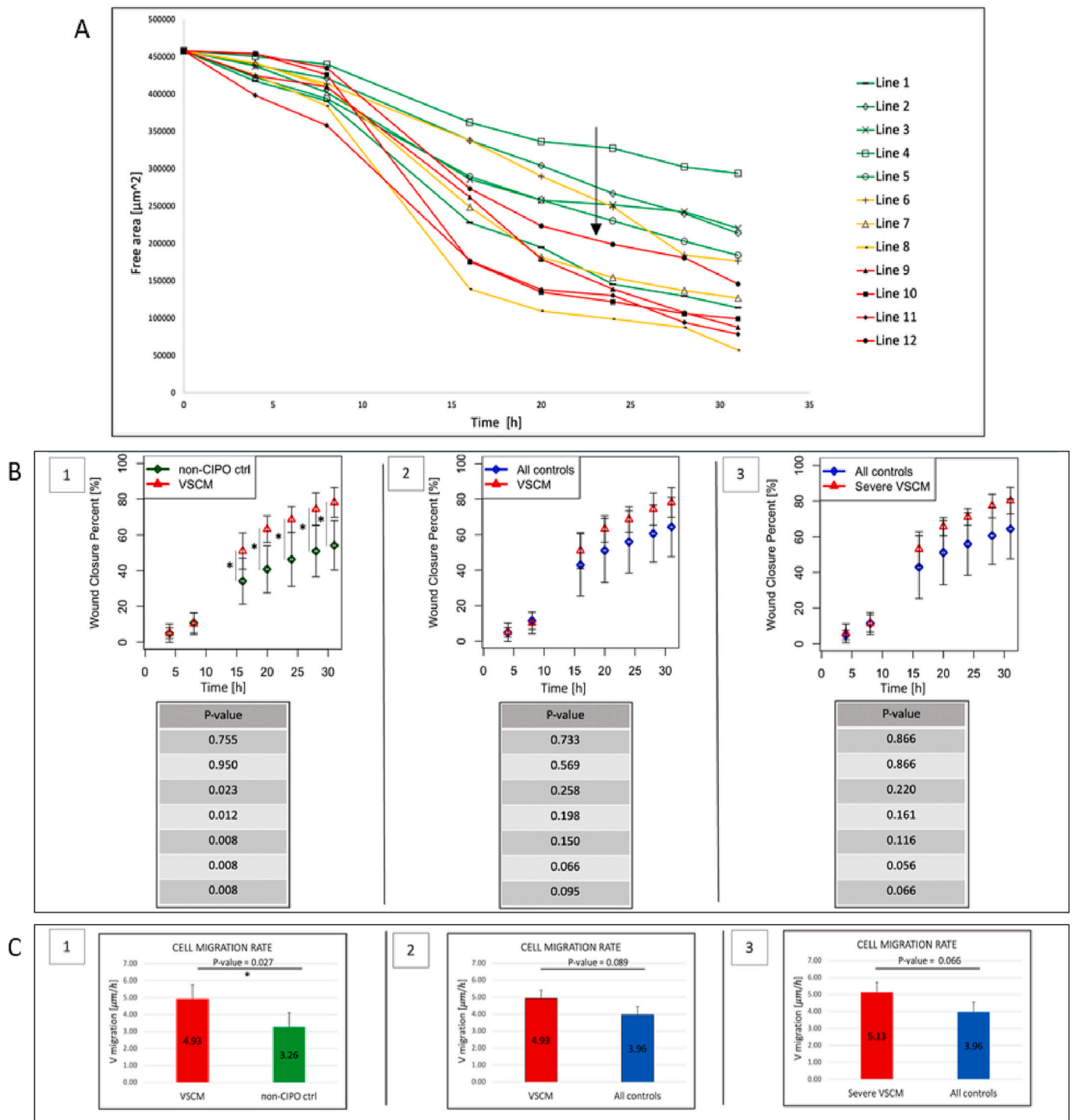
Fig. 2. A. Trend plot of wounds closure during acquisition times. Green lines: control cell lines. Yellow lines: HSCR-affected lines. Red lines: VSCM-affected cell lines. Vertical arrow indicates *ACTG2*[R38H] cell line. B. Percentage of wound closure over time. *P*-values for each time step are reported in table. C. Cell migration rate in different case studies. 'non-CIPO ctrl' = 5 samples; 'HSCR cases' = 3 samples; 'VSCM cases' = 4 samples; 'severe VSCM cases' = 3 samples. Each experiment was performed in 3 replicates. P-value were obtained through Wilcoxon-Mann-Whitney test.

deviation. In order to verify whether the parameters studied were able, with statistical significance and robustness, to distinguish between VSCM cases and controls, null hypothesis tests were performed. If the data satisfied the tests for the normal distribution, the parametric Student's *t*-test was used to compare two populations. If not, nonparametric tests such as the Wilcoxon-Mann–Whitney, the Kolmogorov–Smirnov test, the Kruskal-Wallis tests were applied. Features showing *p*-values <0.05 in population comparisons represent cell phenotypes able of

significantly distinguishing between primary fibroblasts from individuals in different health conditions. In line with the literature on scratch tests [33,40], no corrections were applied to statistics for multiple occurrences of the wound healing assay, whereas Dunn's test was used for multiple comparison in the cell stiffness evaluation of statistical significance.
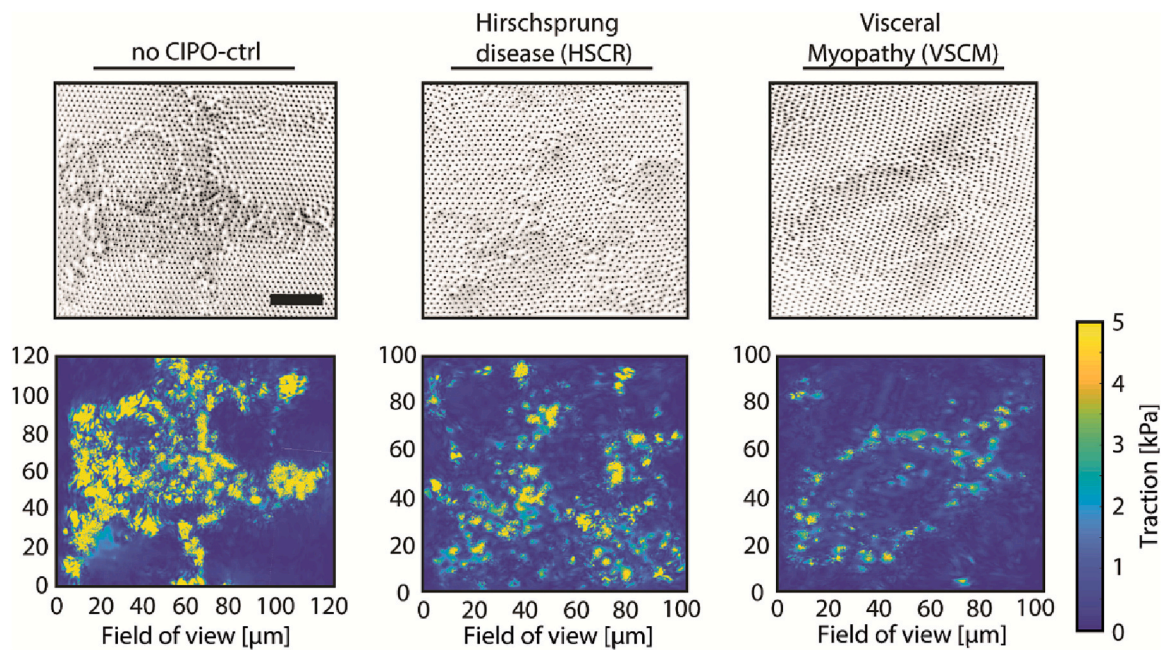
Fig. 3. Representative inverted fluorescent images of quantum dots displaced fields of healthy primary dermal fibroblasts, fibroblasts of patients affected by Hirschsprung disease (HSCR), and fibroblasts of patients affected by Visceral Myopathy (VSCM) (top row); corresponding traction force field map (bottom row). Scale bar 30 μm.

2.9. Study approval

Giannina Gaslini Institute in Genoa (Italy) formulated a written informed consent, shared with patients. It was received from patients or patients' families prior to their participation to the study. The study protocol was approved by the "Comitato Etico Regionale della Liguria" - n. registro CER Liguria: 269/2021 - DB id 11485.

3. Results

Biophysical approaches were applied to assess morphological and mechanical properties of fibroblasts. The values obtained were analyzed in the light of diverse experimental designs, to estimate the adequacy of each parameter in discriminating fibroblasts from VSCM-affected patients and control fibroblasts.
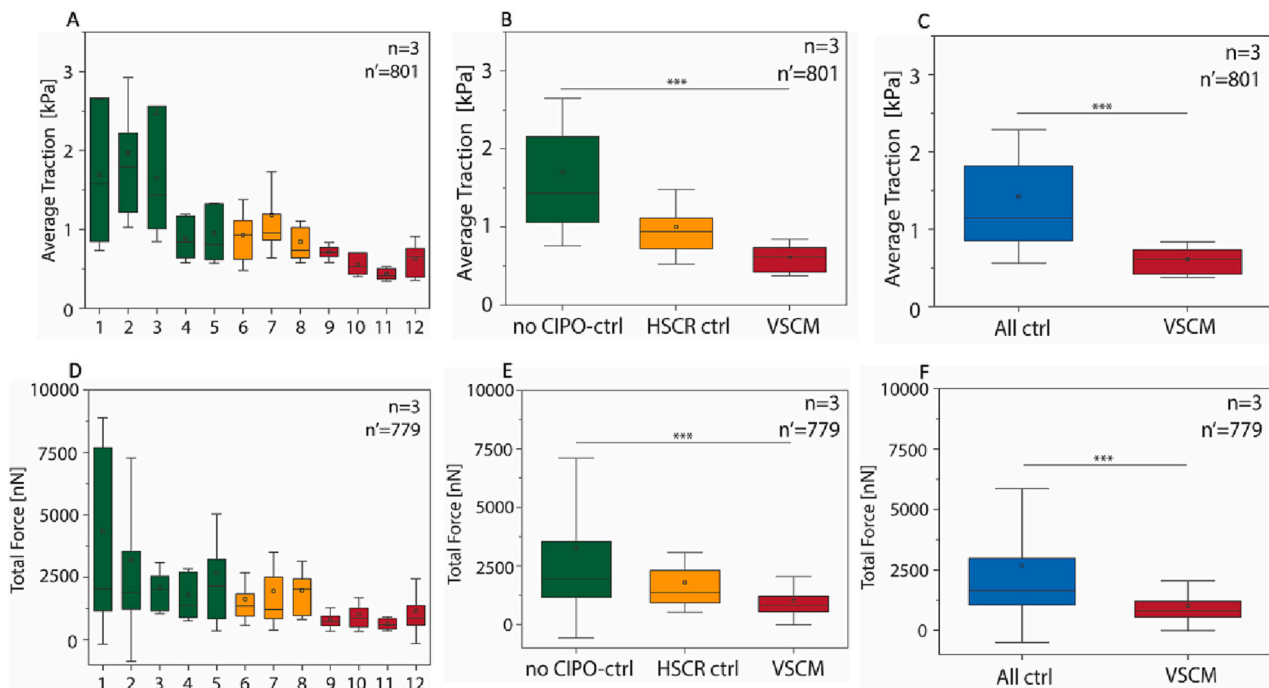

Fig. 4. cTFM data. For all samples (control cell lines in green, VSCM affected cell lines in red, HSCR samples in yellow), as resulting from Cellogram software (A) and normalized by projected cell area (D). For aggregated samples. Non-CIPO control population (green), HSCR control population (yellow), VSCM affected population (red), as resulting from Cellogram software (B) and normalized by projected cell area (E). For all-control population (including HSCR samples, in blue), VSCM affected population, carrying variants in the *ACTG2* gene (either R257C or R38H, in red) as resulting from Cellogram software (C) and normalized by projected cell area (F). Cellogram software [44]. Each experiment was performed in 3 replicates. P-value were obtained through Wilcoxon-Mann-Whitney test.

3.1. Cell mechanical properties

3.1.1. Elasticity

Results related to single cell nanoindentation, to assess the Young's modulus (E) of cells, are reported in Fig. 1. The average values of cellular stiffness settled between 1.4 and 2.2 kPa (Fig. 1A, B). To assess the clustering power of the cell stiffness parameter, values from ACTG2 VSCM cell lines, non-CIPO and HSCR control lines were compared. Such comparison highlighted that cell elasticity value is not able to discriminate VSCM from controls (Fig. 1C). Nevertheless, when comparing controls to severe VSCM cases ($ACTG2^{R257C}$), whole cell stiffness assessed through Hertz model application appears able to significantly distinguishing severe VSCM cases form controls (Fig. 1D), showing *p*-values <0.05 for the three population comparison (p-value = 0.0002 for non-CIPO vs. severe VSCM; p-value = 0.0094 for non-CIPO vs. HSCR; p-value = 0.0103 for HSCR vs. severe VSCM), thus revealing that this parameter can be a meaningful feature to identify severe VSCM cases.

3.1.2. Cell migration

Monitoring cell migration over 31 h showed two main clusters, one including non-CIPO controls (green), characterized by slow migration rates, and the other grouping fibroblasts from VSCM affected patients (red) that migrate more rapidly (Fig. 2A). An exception is represented by cell line 12, which behaves more similarly to healthy controls than to other VSCM affected lines (arrow in Fig. 2A). Interestingly, this fibroblast line carries the $ACTG2^{R38H}$ variant, responsible for a very mild VSCM phenotype [10]. HSCR cases (yellow) are widespread among others, affecting the discrimination power of cell migration-related parameters. Based on these data, the wound closure percentage and the cell migration rate parameters were calculated, and their power in discriminating VSCM from control cells verified. The wound closure percentage over time (Fig. 2B) appears effective in distinguishing VSCM only from non-CIPO controls, during the last five acquisition time points, from 16 h of culture onward (*p*-value <0.05). An analogous level of significance was obtained when studying cell migration rate: a p-value <0.05 was obtained only when comparing VSCM to non-CIPO cell lines (Fig. 2C). Exclusion of the VSCM mild case from statistics did not improve the discriminative power of these two cell features.

3.1.3. Traction force microscopy

To estimate the forces exerted by the cells to the substrate, cells were seeded at low density (initial cell density 1000 cells/cm^2). Individual cells were monitored through live-cell microscopy and the cell-induced displacement of the QDs from their original position in the triangular array was captured (Fig. 3). A finite element analysis of the resulting vectorial displacement field, based on the material model of the substrate [44], resolved the force field maps.

To better show the link between cell lines and force generation, the measured cellular force was divided by the cell basal area to obtain the average traction, for each cell line (Fig. 4A). To assess the effectiveness of cell traction force level in distinguishing VSCM population from controls, Mann-Whitney test was applied to obtain the *p*-value for these non-parametric distributions. Results appeared statistically significant in all population comparisons (Fig. 4B, p-values ≪ 0.01), thus highlighting remarkable differences in the traction force ability of VSCM lines compared to all control lines (Fig. 4C). Statistical significance is confirmed also when considering total force (Fig. 4D-F).

3.2. Morphological assessment

3.2.1. Cell shape

Cell shape was evaluated by holographic microscopy. A total amount of 117 cells from non-CIPO controls, 101 cells from VSCM fibroblasts and 73 cells from HSCR samples were acquired for the analysis. Relying on digital holography, a high number of 2D and 3D morphological features can be assessed, regarding geometric and texture aspects. For
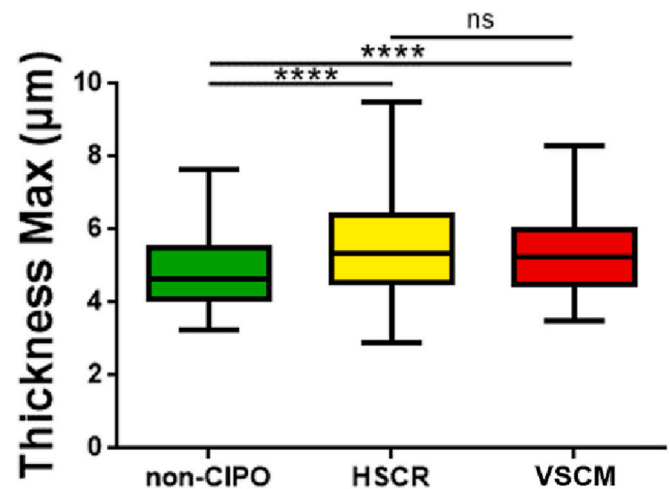

Fig. 5. Test on single cells maximum thickness values shows statistical significance through the Kruskal Wallis non-parametric test, applying Dunn's test for multiple comparison. 'non-CIPO controls' = 117 cells; 'VSCM cases' = 101 cells; 'HSCR cases' = 73 cells.

each feature, the mean value of the distribution and the related standard deviation were obtained (data not shown). Overall, only cell maximum thickness, calculated as the maximum phase shift in the whole selected cell area, appeared able to correctly identify VSCM-affected cell lines. In particular, relying on the one-way non-parametric ANOVA test and applying Dunn's test for multiple comparison, this parameter was able to significantly distinguish VSCM from non-CIPO controls (*p*-value <0.0001), while it could not discriminate between VSCM and HSCR samples (Fig. 5).

3.2.2. Cytoskeletal organization

A morphological analysis of the F-actin was performed, to evaluate the organization of the cytoskeleton structure by observing the whole actin filaments. This was carried out by labelling with Alexa Fluor 647-conjugated phalloidin VSCM-affected and control fibroblasts (Fig. 6A). The analysis concerned the texture and the anisotropy of the cytoskeleton filaments. Texture evaluation relied on Haralick's and Gabor formulas. On this basis, F-actin signal texture features of VSCM fibroblasts did not differ from those of healthy or HSCR cells (Fig. 6B).

The same images were used to assess the F-actin filament orientation by quantifying the cytoskeleton anisotropy for different samples. Number of cells (N) analyzed for each condition were: control samples (N = 112), HSCR samples (N = 43), VSCM samples (N = 53), severe VSCM (N = 32), mild VSCM (N = 21). The anisotropy parameter is able to slightly distinguish the set of VSCM cases from non-CIPO cases (*p*-value <0.05) and, more powerfully, from HSCR controls (Fig. 7A). Furthermore, the anisotropy was able to robustly discriminate the subset of severe VSCM from all controls, while no significant difference was found between the cytoskeletal anisotropy of mild VSCM and controls (Fig. 7B).

When staining cells for gSMA with a specific antibody, the presence of signal spots in cell cytoplasm, resembling gSMA aggregates, could be detected (Fig. 8A). Quantification of spot number by an automated algorithm revealed that two out of three VSCM fibroblasts bearing variants in *ACTG2* displayed a significantly increased number of cytoplasmic gSMA aggregates with respect to non-CIPO controls (Fig. 8B). Interestingly, the same feature was observed in HSCR fibroblasts.

4. Discussion

Gastrointestinal motility disorders, collectively known as Chronic Intestinal Pseudo-Obstruction (CIPO), represent a major medical
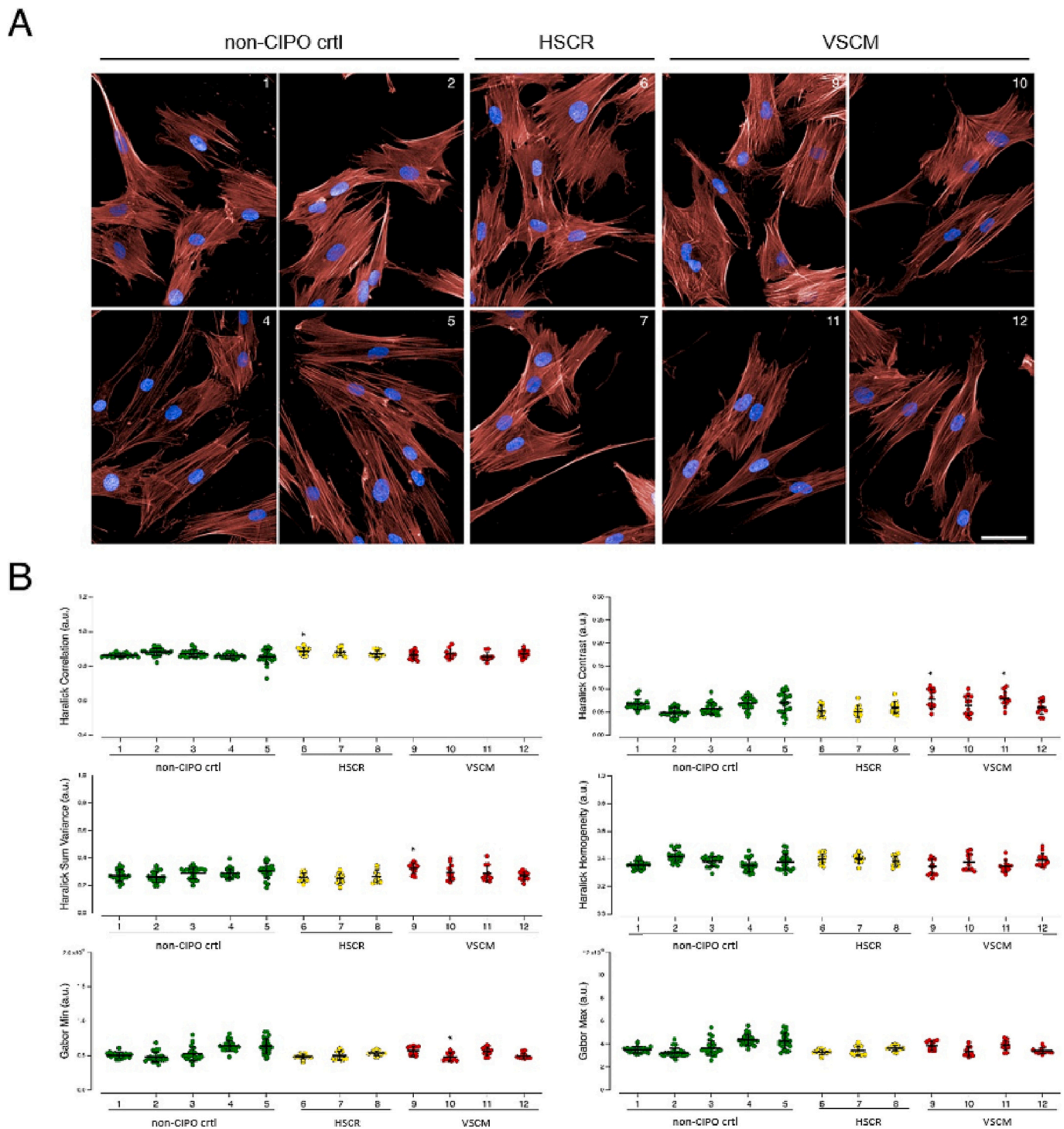
Fig. 6. Texture analysis of F-actin cytoskeleton. A) F-actin cytoskeleton was visualized by staining with phalloidin conjugated with Alexa Fluor 647 in fibroblasts from VSCM patients and controls (healthy subjects and HSCR patients). Scale bar = 100 μm. B) Quantification of cells displaying increased number of gSMA aggregates. Texture analysis was performed according to Gabor's and Haralick's formulas. The graphs show the different parameters calculated for each cell line. Each dot represents the values obtained, for the corresponding parameter, from the analysis of a region measuring 990 × 1320 μm (from independent biological replicates; $n = 6$–12), having similar cell density and distribution. Asterisks indicate statistical significance vs. pooled values of controls: *, $p < 0.05$; **, $p < 0.01$; ***, $p < 0.001$ (Kruskall-Wallis test followed by Dunn's multiple comparison test or parametric ANOVA followed by Dunnet multiple comparison test).

challenge due to diagnostic difficulties (compensated only partially by known genetic etiology), little knowledge about pathogenic mechanisms (preventing effective development of pharmacological treatments), severity of symptoms, and lack of appropriate pharmacological treatments. This complex scenario has prompted the study of the most common myogenic form of CIPO, namely the visceral myopathy

(VSCM), which was associated with specific heterozygous *ACTG2* variants in around 45 % of the patients suffering from generalized failure of visceral smooth muscle contraction, and with variants in other genes of the smooth muscle contraction pathway (*MYH11, MYL9, LMOD1, MYLK*) in around 10 % of cases. The unmet needs related to VSCM represent a heavy load for patients, families, and society. Overall, the
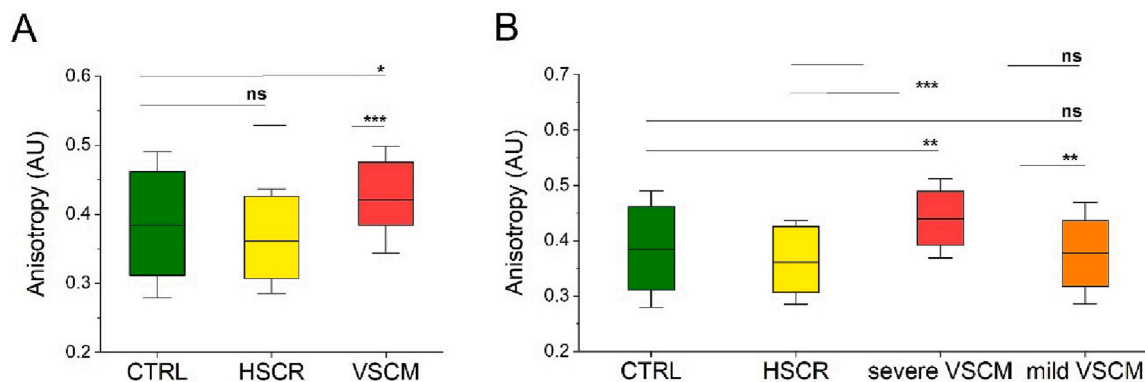
Fig. 7. Anysotropy analysis of F-actin cytoskeleton. A. Anisotropy values for F-actin cytoskeleton. B. Anisotropy values when severe and mild VSCM subsets are separated. Asterisks indicate statistical significance: ns nonsignificant, *p < 0.05, **p < 0.01, ***p < 0.001 (Statistical analysis: two sample *t*-test). CTRL samples (*N* = 112), HSCR samples (*N* = 43), VSCM samples (*N* = 53), severe VSCM (32), mild VSCM (*N* = 21).

current VSCM diagnostic strategy fails to cover approximately 45 % of patients sharing similar symptoms, who cannot receive a certain diagnosis or are misdiagnosed. This translates into their wandering across several clinical screening and hospitals, with crucial delay in enabling the correct management of the pathology and costs for the Health Systems. Advancements in the diagnostic strategy are urgently needed, encompassing the identification of novel markers of disease to integrate the current clinical and genetic evaluations. On the other hand, pharmacological therapy does not exist for VSCM: currently, affected individuals endure prolonged hospitalizations and surgical interventions, often becoming dependent on parenteral nutrition and bladder catheterization, surviving with highly compromised quality of life [55].

In order to dig into the molecular and cellular defects responsible for the VSCM pathogenesis, we performed a wide characterization of patients' dermal fibroblast cells, looking for biomechanical features suitable to distinguish between defective and non-defective cells. The cellular phenotype could integrate and complement clinical and genetic assessment to consolidate the identification of VSCM, even in cases where the genetic outcome cannot directly support the diagnosis of the disease. Dermal fibroblasts can be collected from patients without highly invasive interventions and without compromising the delicate equilibrium of VSCM patients' gut, thus resulting in a procedure that could easily be translated towards a clinically-relevant diagnostic process. To inspect the cellular mechanical phenotype, several morpho-mechanical features of fibroblasts were tested: single cell elasticity, cell population migration, single cell traction forces, two- and three- dimensional cell shape, cytoskeleton organization. The interest in these aspects of the cellular phenotype associated with VSCM lies in the involvement of mechanical issues consistent with the molecular and clinical scenarios of the disease. First, VSCM presents the lack of intestinal contraction as its major symptom, thus possibly involving a mechanical dysfunction at both tissue and cell levels. Second, the genetic variants mostly associated with VSCM were found in *ACTG2*, expressed in enteric smooth muscle cells [56], which is part of the cytoskeleton and therefore involved in cell shape and its mechanical properties. Third, ACTG2 as well as other genes causing VSCM (*MYH11, MYL9, LMOD1, MYLK*) are part of the smooth muscle contraction biological pathway (see https://reactome.org/, identifier: R-HSA-445355), an observation which clearly highlight the involvement of a cell mechanical component in VSCM. Finally, it is emerging that mutant gSMA could affect the F-actin polymerization and/or contribute to abnormal F-actin bundles formation, which reflects on cell shape and mechanical characteristics [3,57].

In the current paper, results of a wide characterization of primary dermal fibroblasts from VSCM affected patients and controls are reported. Other groups [3,56] have recently investigated the morphomechanical features of cells resembling VSCM (through *ACTG2*[R257C] over-expression), showing impairments of cellular biomechanical

features in the presence of *ACTG2* variants. In contrast, the present work relies on patients' primary cells. Working with primary dermal fibroblasts represents an advanced and particularly novel experimental design, especially in the perspective of improving the efficiency of the diagnostic pathway. Indeed, on one hand, patients' primary cells carry the whole machinery leading to the disease phenotype, thus being more representative of the pathology than transfected cells; on the other side, dermal fibroblasts are quite easily accessible and maintainable in biobanks and cell cultures, thus representing a suitable model to implement future VSCM diagnostic and therapeutic strategies.

Our evaluations showed that the ability of cells to contract, tested by traction force microscopy, is clearly impaired in all VSCM patient samples, independently on whether the genetic cause was either *ACTG2*[R257C] or *ACTG2*[R38H] (Fig. 4). Previously, other groups tried to convert the lack of cell contraction ability in a quantitative indicator of the disease, relying on collagen gel cell-contraction assays [56–58]. Working on *ACTG2*[R257C] transfected smooth muscle cells, Hashmi et al. [3] revealed no differences in their contraction ability, compared to wild type cells, differing from our findings. Discordance with our results could be due to different strategies to assess contraction: collagen gel identifies the radial, cumulative contraction of the whole cell population, while cTFM offers a far higher resolution and control on the experimental conditions.

Another mechanical feature that seems defective in primary fibroblasts from VSCM-affected patients is migration. Our wound healing tests showed that *ACTG2*[R257C] samples are able to migrate faster than non-CIPO controls. Interestingly, sample carrying *ACTG2*[R38H] variant showed migration performance similar to controls: this appears in line with clinical evaluations, which associate the *ACTG2*[R38H] variant with mild VSCM symptoms. Results on *ACTG2*[R257C] resemble findings from Hashmi et al. [3] who showed that *ACTG2*[R257C] smooth muscle cells migrated 11 % faster and spread over a 21 % greater area compared to wild-type cells. A decreased cell contraction ability appear in contradiction with the improved cell migration experienced in the presence of *ACTG2*[R257C]. However, the coupling between adhesion forces and migration is a complex mechanism [59], involving different cellular components, as recently suggested for VSCM [3,60].

Since cell stiffness is largely impacted by the organization and structure of actin filaments [61], another interesting feature to test in this context is cell elasticity. Literature shows that cell elasticity consistently correlates with the physiological and pathological state of the cell [62]. Among the methods commonly used to measure mechanical behavior of cells, nanoindentation is by far the most popular to obtain the value of single cell elastic modulus [63]. In our case, the Young modulus of the whole cell, obtained by fitting the forcedisplacement curve with the Hertz model, is able to distinguish VSCM samples from controls only when considering severe VSCM cases.
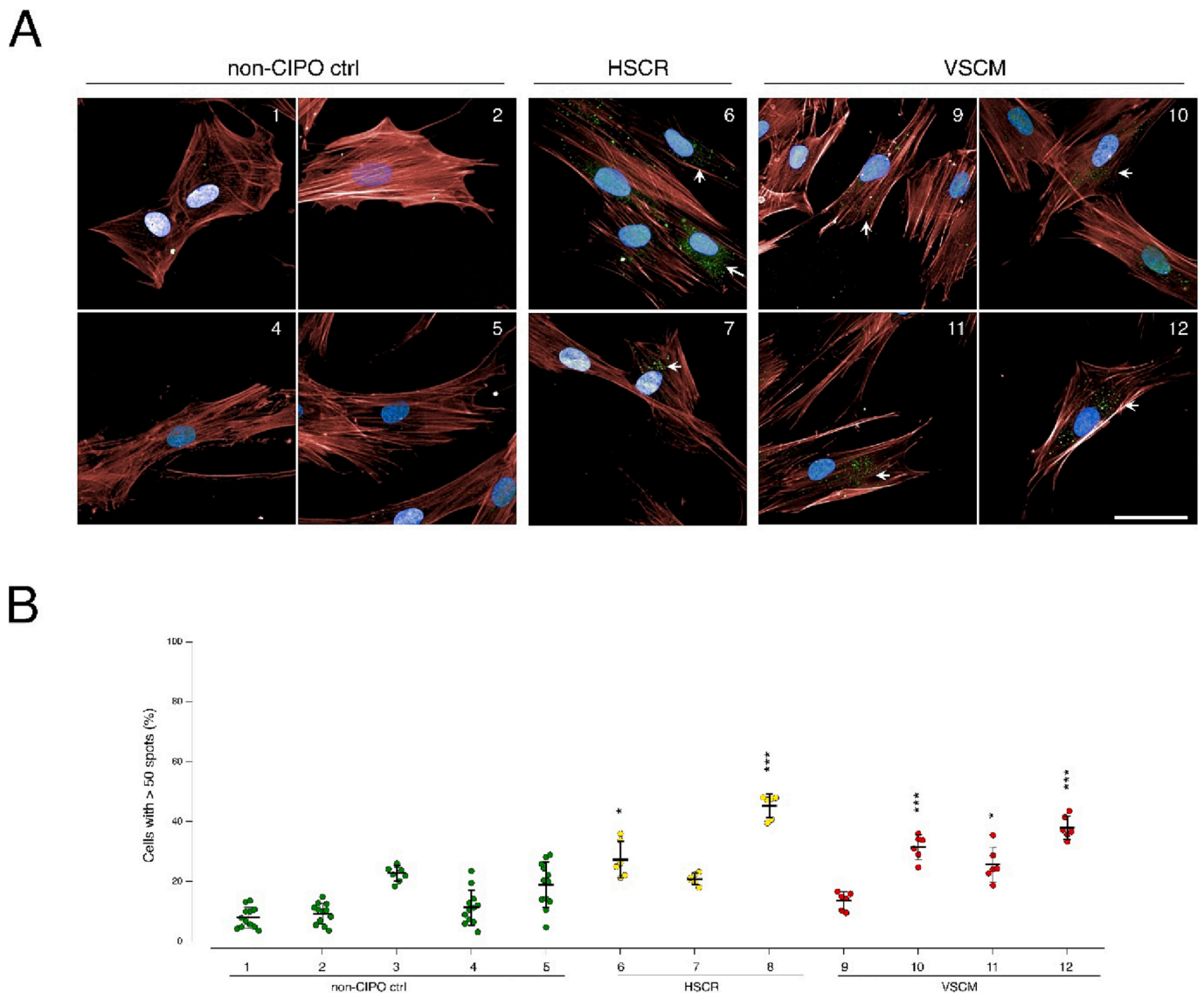
Fig. 8. Analysis of *ACTG2* expression. A. Immunolocalization of gSMA in fibroblasts from VSCM patients and controls (non-CIPO and HSCR subjects). gSMA was visualized using an anti-ACTG2 antibody followed by a secondary antibody conjugated with Alexa Fluor 488. The F-actin cytoskeleton was visualized by staining with phalloidin conjugated with Alexa Fluor 647. The immunostaining highlighted the presence of spots (see arrows), resembling putative gSMA aggregates, whose number was significantly increased in fibroblasts from VSCM and HSCR subjects. Scale bar = 50 μm. B. Quantification of cells displaying increased number of gSMA aggregates. Each dot represents the values obtained from the analysis of a region measuring 990 × 1320 μm (from independent biological replicates; n = 6–12), having similar cell density and distribution. Asterisks indicate statistical significance vs. pooled values of controls: *, $p < 0.05$; **, $p < 0.01$; ***, $p < 0.001$ (Kruskall-Wallis test followed by Dunn's multiple comparison test).

Nevertheless, the Young's modulus is a bulk feature, accounting for the contribution from the entire cell and this might confound the interpretation of the results. In particular, considering the pivotal role of actin in VSCM, it may be interesting to analyze the elasticity of the cell cortex, which is predominantly composed by actin, by using more detailed models that can isolate the contribution of this component [62].

Regarding cell shape, holography allowed us to assess 2D and 3D cellular features in label free conditions. The whole set of 32 parameters evaluated by the HStudio software were considered to assess whether the features of the shape of adherent cells could represent a biomarker of pathology. Only maximum thickness of plated cells arose as a characteristic able to significantly distinguish between the group of affected samples and the set of controls (Fig. 5).

Finally, we studied the organization of cytoskeletal fibers, which could reveal useful aspects to improve both the diagnostic path and the design of novel hypothesis on about the molecular mechanism underlying this disorder. Other groups investigated F-actin polymerization in

the presence of *ACTG2* variants, with different findings. Through fluorescence on cell culture and co-sedimentation approaches, Halim et al. [56] showed that, while wild-type gSMA could be incorporated into the actin filaments, no co-localization was observed with gSMA in the presence of R178C, R178L, R178H, R40C, R63Q, R148S variants, potentially reflecting impaired actin polymerization and changes in the overall actin organization. Analogous conclusions for R148S variant had already been drawn by Lehtonen et al. [57], whose results are, at least partially, in line with our present observations. By co-staining gSMA and F-actin in fibroblasts, we did not identify any localization of gSMA in the actin filaments, while peculiar dots of gSMA were identified in a statistically significant quantity in 2 out of 4 VSCM and 2 out of 3 HSCR cell lines. We could not ascertain any correlation between F-actin texture and the presence of gSMA aggregate structures in fibroblasts. If these spots reflect the presence of putative gSMA aggregates in VSCM cases, possibly accounting for the misfolding of the gSMA protein due to gene variants, it cannot be easily explained for HSCR fibroblasts, which do not
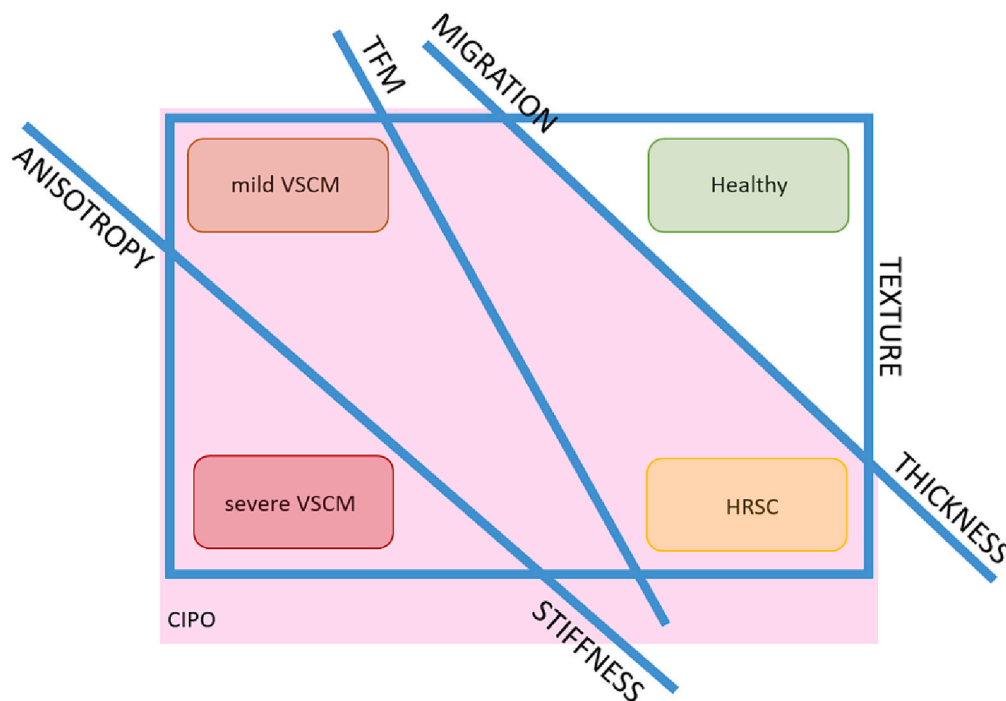
Fig. 9. Overall schema of the ability of the tested morpho-mechanical features in discriminating VSCM fibroblasts from controls.

carry any cytoskeletal protein defect. Therefore, this aspect needs further investigations, since also disease-independent conditions such as cell cycle, culture confluency or cell differentiation state might influence the presence of dots.

By using transmission electron microscopy, Collins et al. [65] found disorganized aggregates of 9- to 11-nm actin filaments in smooth muscle cells from a patient carrying the *ACTG2*^{G147C} variant. Working on *ACTG2*^{R257C} smooth muscle cells, fluorescently labelling gSMA and f-actin, Hashmi et al. [3] found no profound disruption of the overall organization of the actin cytoskeletal networks in mutant compared to wild-type cells. On the other hand, they found differences in filament structure: gSMA carrying the R257C variant was incorporated into fewer, shorter, thinner, and less branched F-actin bundles compared to the wild-type protein. This is in line with our findings, since we also found partial differences in filament structures of VSCM and controls fibroblasts. In fact, although actin filaments of VSCM cells appear to be indistinguishable from controls in terms of cytoskeletal texture, and no peculiar pattern seems to be associated with affected cells, the measure of the anisotropy of the cytoskeletal fibers has revealed differences between severe VSCM and control cell lines. Interestingly, mild VSCM (associated with the *ACTG2*^{R38H} variant) appeared to behave as the controls.

The evaluation of cellular morpho-mechanical characteristics of primary fibroblasts from patients carrying genetic variants associated with VSCM (i.e. *ACTG2*^{R257C} and *ACTG2*^{R38H}) revealed differences that could be powerful in discriminating between sets of different group of individuals. With the exception of cytoskeletal texture, which proved unable to distinguish the VSCM group from controls, all the other cell features were successful, at different degree, in separating different patient and control sets (Fig. 9). In particular, cell stiffness and cytoskeletal anisotropy were able to identify fibroblasts from severe VSCM cases among any other fibroblast line. Cell migration and cell maximum thickness were less powerful, being able to separate CIPO from non-CIPO cases, suggesting that these features are likely not directly related to the mechanical impairment in VSCM due to *ACTG2* genetic variants. Traction force microscopy was the test that better than any other approach is able to discriminate myopathic CIPO form all controls.

These findings could prove to be powerful biomarkers of pathology.

In particular, with a view to improve the diagnosis of the disease even when no genetic variant potentially responsible of the disease is detected, cellular phenotypic markers could support the current assessments.

Moreover, the identified cell phenotype approaches could be exploited also in light of enabling therapeutic strategy. In fact, they can be used as functional tests to evaluate the effectiveness of candidate drugs in restoring a physiological phenotype of VSCM affected cells.

In conclusion, several important take-home messages emerge from this study. First, *we identified a new model of disease*. Dermal fibroblasts represent a reliable and manageable model for the study of VSCM. We have demonstrated that, although expressed at low level in fibroblasts, *ACTG2* variants appear to induce modifications in the cellular phenotype. Hence, dermal fibroblasts could be potentially useful to set-up specific tests based on cell biomechanics and biophysical properties, to support the current VSCM diagnostic procedure. Interestingly, donors age seems not to impact dramatically on fibroblasts behavior: control samples, which come from both pediatric and young-adult subjects, show similar biomechanical features (Figs. 1, 2, 4, 6, 8). Second, *we discovered that cell mechanical features can support R257C-ACTG2-based VSCM diagnosis and therapy identification*. Some of the cellular biomechanics parameters considered here (i.e. cell traction force, cell stiffness and cytoskeletal anisotropy) have turned out to be particularly suitable to discriminate between fibroblasts from patients carrying ACTG2^{R257C} mutant and controls, with potential benefits on diagnostic protocols, especially when a disease-associated causative mutation is missing. Moreover, the identified morpho-mechanical cell features can be used in functional tests for identifying molecules effective for reducing the mechanical impairment caused by VSCM. Third, *our results support the hypothesis that ACTG2*^{R257C} *mutant could alter cytoskeleton organization*. Literature data on the effects of *ACTG2* variants on actin polymerization have not achieved a consensus yet, although cytoskeleton could be primarily affected in *ACTG2*-mediated forms of VSCM. This might be due to the use of different experimental models, such as different cell lines, and to the evaluation of different *ACTG2* variants, that could realistically lead to diverse levels of impairments on actin bundles, as reflected at disease symptom level. Nevertheless, different studies, including ours, consistently show evidence that, in the presence of *ACTG2*^{R257C} variant, the structure of actin filaments network could be

deformed with respect to controls.

Many aspects remain elusive in VSCM. Further investigations at the cellular and tissue level will represent a step towards for improving the knowledge on this pathology and the life condition of patients. Nevertheless, the present study can contribute to improve the effectiveness of diagnostic strategies for VSCM and pave the road for the identification of still missing pharmacological treatments, especially for ACTG2^{R257C}-based form of the disease.

CRediT authorship contribution statement

FV and IC conceived the idea and supervised the work. FMP, BDM and CG performed traction force experiments. MM and FB contributed to wound healing assay tests. RM contributed to wound healing assay and traction force microscopy tests. NP, FCZ and VT performed cytoskeletal analysis. MA, MZ, TF and MV contributed to stiffness tests. GS isolated fibroblasts from skin samples, provided genetic characterization of fibroblasts lines and preserved them in biobank. PG provided information on patients as well as blood and the skin specimens for genetic tests and cell culture setup. MN and AB performed molecular biology tests. SS carried out cell biology tests. All coauthors contributed to revise the manuscript.

Declaration of competing interest

The authors declare the following financial interests/personal relationships which may be considered as potential competing interests: Federica Viti reports financial support was provided by Fondazione Alessandra Bono. Isabella Ceccherini reports financial support was provided by Fondazione Alessandra Bono. Costanza Giampietro reports financial support was provided by Swiss National Science Foundation.

Data availability

No data was used for the research described in the article.

Acknowledgement

Appendix A. Supplementary data

Supplementary data to this article can be found online at https://doi.org/10.1016/j.bioadv.2023.213355.

References

[1] C.H. Knowles, et al., The London classification of gastrointestinal neuromuscular pathology: report on behalf of the gastro 2009 international working group, Gut 59 (2010) 882–887.

[2] E. Perez de Arce, et al., Chronic intestinal pseudo-obstruction: clinical and manometric characteristics in the chilean population, J. Neurogastroenterol. Motil. 23 (2) (2017) 273–280.

[3] S.K. Hashmi, et al., Pseudo-obstruction-inducing ACTG2(R257C) alters actin organization and function, JCI Insight 5 (16) (2020), e140604.

[4] W.E. Berdon, et al., Megacystis microcolon intestinal hypoperistalsis syndrome: a new cause of intestinal obstruction in the newborn. Report of radiologic findings in five newborn girls, Am. J. Roentgenol. 126 (1976) 957–964.

[5] M.F. Wangler, A.L. Beaudet, ACTG2-related disorders, in: R.A. Pagon, M.P. Adam, H.H. Ardinger, et al. (Eds.), GeneReviews® [Internet], University of Washington, Seattle, Seattle (WA), 2015, pp. 1993–2016.

[6] N. Assia Batzir, et al., Recurrent arginine substitutions in the ACTG2 gene are the primary driver of disease burden and severity in visceral myopathy, Hum. Mutat. 41 (3) (2020) 641–654.

[7] D.M. Milewicz, et al., De novo ACTA2 mutation causes a novel syndrome of multisystemic smooth muscle dysfunction, Am. J. Med. Genet. A 152A (10) (2010 Oct) 2437–2443.

[8] M.A.T. Bortolini, et al., Expression of genes encoding smooth muscle contractile proteins in vaginal tissue of women with and without, Neurourol. Urodyn. 31 (2012) 109–114.

[9] I. Matera, et al., Novel ACTG2 variants disclose allelic heterogeneity and bi-allelic inheritance in pediatric chronic intestinal pseudo-obstruction, Clin. Genet. 99 (3) (2021) 430–436.

[10] I. Matera, et al., Variants of the ACTG2 gene correlate with degree of severity and presence of megacystis in chronic intestinal pseudo-obstruction, Eur. J. Hum. Genet. 24 (8) (2016) 1211–1215.

[11] A. Milunsky, et al., Diagnosis of chronic intestinal pseudo-obstruction and megacystis by sequencing the ACTG2 gene, J. Pediatr. Gastroenterol. Nutr. 65 (4) (2017) 384–387.

[12] J. Gauthier, et al., A homozygous loss-of-function variant in MYH11 in a case with megacystis-microcolon-intestinal hypoperistalsis syndrome, Eur. J. Hum. Genet. 23 (9) (2015) 1266–1268.

[13] C.A. Moreno, et al., Homozygous deletion in MYL9 expands the molecular basis of megacystis-microcolon-intestinal hypoperistalsis syndrome, Eur. J. Hum. Genet. 26 (5) (2018) 669–675.

[14] D. Halim, et al., Loss-of-function variants in MYLK cause recessive megacystis microcolon intestinal hypoperistalsis syndrome, Am. J. Hum. Genet. 101 (1) (2017) 123–129.

[15] D. Halim, et al., Loss of LMOD1 impairs smooth muscle cytocontractility and causes megacystis microcolon intestinal hypoperistalsis syndrome in humans and mice, Proc. Natl. Acad. Sci. U. S. A. 114 (13) (2017) E2739–E2747.

[16] C.T. Lim, A. Li, Mechanopathology of red blood cell diseases — why mechanics matters, Theor. Appl. Mech. Lett. 1 (1) (2011), 014000.

[17] A. Mescola, et al., Probing cytoskeleton organisation of neuroblastoma cells with single-cell force spectroscopy, J. Mol. Recognit. 25 (5) (2012) 270–277.

[18] C.W. Lee, et al., Membrane roughness as a sensitive parameter reflecting the status of neuronal cells in response to chemical and nanoparticle treatments, J. Nanobiotechnol. 14 (2016) 9.

[19] J.M. Northcott, et al., Feeling stress: the mechanics of cancer progression and aggression, Front. Cell Dev. Biol. 6 (2018) 17.

[20] N. Scholz, Cancer cell mechanics: adhesion G protein-coupled receptors in action? Front. Oncol. 8 (2018) 59.

[21] M.J. Harris, D. Wirtz, P.H. Wu, Dissecting cellular mechanics: Implications for aging, cancer, and immunity, Semin. Cell Dev. Biol. 93 (2019) 16–25, https://doi.org/10.1016/j.semcdb.2018.10.008. Sep; Epub 2018 Oct 30. PMID: 30359779.

[22] J. Zemla, et al., Atomic force microscopy as a tool for assessing the cellular elasticity and adhesiveness to identify cancer cells and tissues, Semin. Cell Dev. Biol. 73 (2018) 115–124.

[23] A.I. Baba, C. Câtoi, Tumor Cell Morphology In: Comparative Oncology, Chapert 3. Available from, The Publishing House of the Romanian Academy, Bucharest, 2007, https://www.ncbi.nlm.nih.gov/books/NBK9553/.

[24] L. Petecchia, et al., A biophysical approach to quantify skeletal stem cells trans-differentiation as a model for the study of osteoporosis, Biophys. Chem. 229 (2017) 84–92.

[25] M.M. Alves, et al., Contribution of rare and common variants determine complex diseases-Hirschsprung disease as a model, Dev. Biol. 382 (1) (2013) 320–329.

[26] J.M. Tilghman, et al., Molecular genetic anatomy and risk profile of Hirschsprung's disease, N. Engl. J. Med. 380 (15) (2019) 1421–1432.

[27] D. Chavan, et al., Ferrule-top nanoindenter: an optomechanical fiber sensor for nanoindentation, Rev. Sci. Instrum. 83 (11) (2012 Nov), 115110.

[28] G. Ciccone, et al., Experimental and data analysis workflow for soft matter nanoindentation, J. Vis. Exp. (2022) 179. Jan 18.

[29] A. Bartolozzi, et al., Development of label-free biophysical markers in osteogenic maturation, J. Mech. Behav. Biomed. Mater. 103 (2020), 103581.

[30] H. Hertz, Über die berührung fester elastischer Körper (On the contact of rigid elastic solids), in: Jones, Schott (Eds.), Miscellaneous Papers 92, J. Reine und Angewandte Mathematik, Macmillan, London, 1896, p. 156, pii: S1084-9521(18) 30143-5.

[31] I. Manika, J. Maniks, Effect of substrate hardness and film structure on indentation depth criteria for film hardness testing, J. Phys. D. Appl. Phys. 41 (2008), 074010.

[32] https://zenodo.org/record/4508646#.YsKHd3ZBxPY.

[33] J. Pijuan, et al., In vitro cell migration, invasion, and adhesion assays: from cell imaging to data analysis, Front. Cell Dev. Biol. 14 (7) (2019 Jun) 107.

[34] A. Azuma, et al., 2'-C-cyano-2'-deoxy-1-beta-D-arabino-pentofuranosylcytosine: a novel anticancer nucleoside analog that causes DNA strand breaks and G(2) arrest, Mol. Pharmacol. 59 (4) (2001 Apr) 725–731.

[35] A.G. Lipman, Martindale — the Extra Pharmacopoeia (30th ed), edited by J. E. F. Reynolds, International Journal of Pharmacy Practice 2 (1993), https://doi.org/10.1111/j.2042-7174.1993.tb00740.x, 124-124.

[36] S.Y. Boateng, et al., Inhibition of fibroblast proliferation in cardiac myocyte cultures by surface microtopography, Am. J. Physiol. Cell Physiol. 285 (2003) C171–C182.

[37] I. Asimov, Data for biochemical research, J. Chem. Educ. 37 (8) (1960) A490.

[38] J.E.N. Jonkman, et al., An introduction to the wound healing assay using live-cell microscopy, Cell Adhes. Migr. 8 (5) (2014) 440–451.

[39] A. Suarez-Arnedo, F. Torres Figueroa, C. Clavijo, P. Arbeláez, J.C. Cruz, C. Muñoz-Camargo, An image J plugin for the high throughput image analysis of in vitro scratch wound healing assays, PLoS One 15 (7) (2020), e0232565, https://doi.org/10.1371/journal.pone.0232565. Jul 28; PMID: 32722676; PMCID: PMC7386569.

[40] A. Grada, et al., Research techniques made simple: analysis research techniques made simple: analysis healing assay, J Invest Dermatol. 137 (2017) e11–e16.

[41] M. Bergert, et al., Confocal reference free traction force microscopy, Nat. Commun. 7 (2016) 12814.

[42] P. Galliker, et al., Direct printing of nanostructures by electrostatic autofocussing of ink nanodroplets, Nat. Commun. 3 (2012) 890.

[43] A.M. Reyes Lua, et al., Factors influencing the mechanical properties of soft elastomer substrates for traction force microscopy, Mech. Soft Mater. 2 (1) (2020) 6.

[44] T. Lendenmann, et al., Cellogram: on-the-fly traction force microscopy, Nano Lett. 19 (10) (2019) 6742–6750.

[45] M. Bergert, et al., Confocal reference free traction force microscopy, Nat. Commun. 7 (2016) 12814.

[46] M. Panagiotakopoulou, et al., Cell cycle-dependent force transmission in cancer cells, Mol. Biol. Cell 29 (21) (2018) 2528–2539.

[47] L. Kyeo Reh, et al., Quantitative phase imaging techniques for the study study of cell pathophysiology: from principles to applications, Sensors 13 (4) (2013) 4170–4191.

[48] M. Schürmann, et al., Refractive index measurements of single, spherical cells using digital holographic microscopy, Methods Cell Biol. 125 (2015) 143–159.

[49] F. Palacios, et al., in: Emilia Mihaylova (Ed.), Holography - Basic Principles and Contemporary Applications, Phase and Polarization Contrast Methods by Use of Digital Holographic Microscopy: Applications to Different Types of Biological Samples, IntechOpen, 2013, pp. 353–377.

[50] B. Rappaz, et al., Digital holographic microscopy: a quantitative label-free microscopy technique for phenotypic screening, Comb. Chem. High Throughput Screen. 17 (1) (2014) 80–88.

[51] R.M. Haralick, et al., Textural features for image classification, IEEE Trans. Syst. Man Cybern. 3 (1973) 610–621.

[52] M.R. Turner, Texture discrimination by Gabor functions, Biol. Cybern. 55 (1986) 71–82.

[53] A. Boudaoud, et al., FibrilTool, an ImageJ plug-in to quantify fibrillar structures in raw microscopy images, Nat. Protoc. 9 (2) (2014) 457–463.

[54] M. Louveaux, et al., The impact of mechanical compression on cortical microtubules in Arabidopsis: a quantitative pipeline, Plant J. 88 (2016) 328–342.

[55] N.S. Dreyer, et al., Rare case of visceral myopathy, J Surg Case Rep 2021 (12) (2021), rjab554.

[56] D. Halim, et al., ACTG2 variants impair actin polymerization in sporadic megacystis microcolon intestinal hypoperistalsis syndrome, Hum. Mol. Genet. 25 (3) (2016) 571–583.

[57] H.J. Lehtonen, et al., Segregation of a missense variant in enteric smooth muscle actin g-2 with autosomal dominant familial visceral myopathy, Gastroenterology 143 (2012) 1482–1491. PMID:22960657.

[58] W. Thorson, et al., De novo ACTG2 mutations cause congenital distended bladder, microcolon, and intestinal hypoperistalsis, Hum. Genet. 133 (6) (2014) 737–742.

[59] L. Yao, Y. Li, Effective force generation during mammalian cell migration under different molecular and physical mechanisms, Front. Cell Dev. Biol. 10 (2022), 903234.

[60] B.D. Southern, et al., Matrix-driven myosin II mediates the pro-fibrotic fibroblast phenotype, J. Biol. Chem. 291 (12) (2016) 6083–6095.

[61] K.E. Kasza, et al., Actin filament length tunes elasticity of flexibly cross-linked actin networks, Biophys. J. 99 (4) (2010) 1091–1100.

[62] P.D. Garcia, R. Garcia, Determination of the elastic moduli of a single cell cultured on rigid support by force microscopy, Biophys. J. 114 (2018) 2923–2932.

[63] Z.L. Zhou, et al., Reliable measurement of elastic modulus of cells by nanoindentation in an atomic force microscope, J. Mech. Behav. Biomed. Mater. 8 (2012) 134–142.

[65] R.R.J. Collins, et al., ACTG2-associated visceral myopathy with chronic intestinal pseudoobstruction, intestinal malrotation, hypertrophic pyloric stenosis, choledochal cyst, and a novel missense mutation, Int. J. Surg. Pathol. 27 (1) (2019) 77–83.